Single-particle density matrix and the momentum distribution of dark "solitons" in a Tonks-Girardeau gas

Buljan, Hrvoje; Lelas, Karlo; Pezer, Robert; Jablan, Marinko

Single-particle density matrix and the momentum distribution of dark "solitons" in a Tonks-Girardeau gas

H. Buljan,[1] K. Lelas,[1] R. Pezer,[2] and M. Jablan[1]

[1]*Department of Physics, University of Zagreb, PP 332, Zagreb, Croatia*
[2]*Faculty of Metallurgy, University of Zagreb, Aleja narodnih heroja 3, Sisak, Croatia*

We study the reduced single-particle density matrix (RSPDM), the momentum distribution, and natural orbitals and their occupancies of dark "soliton" (DS) states in a Tonks-Girardeau gas. DS states are specially tailored excited many-body eigenstates, which have a dark solitonic notch in their single-particle density. The momentum distribution of DS states has a characteristic shape with two sharp spikes. We find that the two spikes arise due to the high degree of correlation observed within the RSPDM between the mirror points (x and $-x$) with respect to the dark notch at $x=0$; the correlations oscillate rather than decay as the points x and $-x$ are being separated.

PACS number(s): 03.75.Kk

I. INTRODUCTION

Exactly solvable models have the possibility of providing important insight into the quantum many-body physics beyond various approximation schemes. Two such models, the Tonks-Girardeau [1] and the Lieb-Liniger model [2], which describe interacting Bose gases in one dimension (1D), have drawn considerable attention in recent years with the developments of experimental techniques for tightly confining atoms in effectively 1D atomic waveguides [3–6]. The Lieb-Liniger (LL) model describes a system of bosons interacting via two-body δ-function interactions [2]. The Tonks-Girardeau (TG) model corresponds to infinitely repulsive ("impenetrable core") bosons in 1D [1,7]; this model is exactly solvable via Fermi-Bose mapping, which relates the TG gas to a system of noninteracting spinless fermions in 1D [1]. A study of atomic scattering for atoms confined transversally in an atomic waveguide has led to a suggestion for the experimental observation of a TG gas [8]; such atomic systems enter the TG regime at low temperatures, low linear densities, and strong effective interactions [8–10]. The experimental realization of the TG model was reported in two experiments from 2004 [4,5]. Moreover, the nonequilibrium dynamics of the 1D interacting Bose gases including the TG regime has been recently experimentally studied within the context of relaxation to an equilibrium [4]. Within this paper we analyze the reduced single-particle density matrix (RSPDM) and related observables of certain specially tailored excited eigenstates of the TG gas, which are also referred to as dark "soliton" (DS) states [11–13].

Dark solitons are fundamental nonlinear excitations. Within the context of interacting Bose gases, they were mainly studied in the regime of weak repulsive interactions [14–17] where mean-field theories [e.g., the Gross-Pitaevskii theory, which employs the nonlinear Schrödinger equation (NLSE)] are applicable. In the regime of strong repulsive interactions in quasi-1D geometry, dark solitons were also studied by using the NLSE with a quintic nonlinear term [18–20]. In Ref. [11], Girardeau and Wright have studied the concept of dark solitons within the exactly solvable TG model; they found specially tailored excited many-body

eigenstates of the TG gas on the ring (DS states), with a dark notch in their single-particle density, which is similar to the dark notch of nonlinear dark solitons. The dynamics of such excitations in a TG gas was studied by Busch and Huyet [12] in a harmonic trap. Recently, a scheme based on parity-selective filtering ("evaporation") of a many-body wave function was suggested [13] as a candidate for the experimental observation of DS states. However, to the best of our knowledge, the momentum distribution, the RSPDM, and natural orbitals (NOs) and their occupancies have not been studied yet for DS states. These quantities are important for a better understanding of DS states, but may also be necessary ingredients for their experimental detection, which provides a motivation for this study.

The calculation of correlation functions (such as the RSPDM) for 1D Bose gases [21–43] from many-body wave functions [1,2,11,44–46] yields important physical information (such as the momentum distribution) on the state of the system. Within the TG model, the RSPDM and the momentum distribution have been studied in the continuous [21,23,24,27,28,32,35,40,43] and discrete (lattice) [31,34,38,39,47] cases, both for the static [21,23,24,27,28,31,32,38,43] and for time-dependent [34,35,39,40] problems. In the stationary case, most studies consider the ground-state properties of the TG gas. The momentum distribution for the ground-state of the TG gas on the ring has a spike at $k=0$, $n_B(k) \propto |k|^{-1/2}$ [21]. In both the harmonic confinement [24,26] and on the ring [26], the TG ground-state momentum distribution decays as a power law $n_B(k) \propto k^{-4}$; in Ref. [26], it has been pointed out that k^{-4} decay is also valid for the LL gas (for any strength of the interaction). These ground states of the TG gas are not Bose condensed [21,28], which is evident from the fact that the occupancy of the leading natural orbital scales as $\sqrt{N}$ for large N [27,28]. In the box confinement, the momentum distribution of a TG gas has been studied by generalizing the Haldane's harmonic-fluid approach [25]. Besides for the ground states, the momentum distribution has been analyzed in time-dependent problems including irregular dynamics on the ring [33], in dynamics in the harmonic potential with time-dependent frequency [35], and in a periodic potential in

the context of many-body Bragg reflections [40]. A number of interesting results for time-dependent problems have been recently obtained within the discrete lattice model including fermionization of the momentum distribution during 1D free expansion [34] and relaxation to a steady state carrying memory of initial conditions [39].

The correlation functions for TG and LL models were studied by using various analytical and numerical methods [21–43]. The formula that was derived and employed in Ref. [40] allows efficient and exact numerical calculation of the RSPDM for the TG gas in versatile states (ground state, excited eigenstates, time-evolving states [40]) and for a fairly large number of particles. We find it suitable for this study of DS states.

Here we numerically calculate the RSPDM correlations, natural orbitals and their occupancies, and the momentum distribution of DS states. We find that these excited eigenstates of a TG gas have the characteristic shape of the momentum distribution with two sharp spikes. The two sharp spikes arise due to the high degree of correlation observed within the RSPDM between the mirror points x and $-x$ with respect to the dark notch at $x=0$; interestingly, the correlations oscillate rather than decay as the points x and $-x$ are being separated.

II. MODEL

We study a system of N identical Bose particles in 1D space, which experience an external potential $V(x)$. The bosons interact with impenetrable pointlike interactions [1], which is most conveniently represented as a subsidiary condition on the many-body wave function [1]:

$$\psi_B(x_1, x_2, \ldots, x_N, t) = 0 \quad \text{if } x_i = x_j \tag{1}$$

for any $i \neq j$. Besides this condition, ψ_B obeys the Schrödinger equation

$$i\frac{\partial \psi_B}{\partial t} = \sum_{j=1}^{N} \left[-\frac{\partial^2}{\partial x_j^2} + V(x_j) \right] \psi_B; \tag{2}$$

here, we use dimensionless units as in Ref. [13]—i.e., $x = X/X_0$, $t = T/T_0$, and $V(x) = U(X)/E_0$, where X and T are space and time variables in physical units, and X_0 is an arbitrary spatial length scale (e.g., $X_0 = 1$ μm), which sets the time scale $T_0 = 2mX_0^2/\hbar$, and energy scale $E_0 = \hbar^2/(2mX_0^2)$; m denotes particle mass, and $U(X)$ is the potential in physical units. The wave functions are normalized as $\int dx_1 \cdots dx_N |\psi_B(x_1, x_2, \ldots, x_N, t)|^2 = 1$.

The solution of this system may be written in compact form via the famous Fermi-Bose mapping, which relates the TG bosonic wave function ψ_B to an antisymmetric many-body wave function ψ_F describing a system of noninteracting spinless fermions in 1D [1]:

$$\psi_B = A(x_1, \ldots, x_N)\psi_F(x_1, x_2, \ldots, x_N, t). \tag{3}$$

Here

$$A = \prod_{1 \leqslant i < j \leqslant N} \text{sgn}(x_i - x_j) \tag{4}$$

is a "unit antisymmetric function" [1], which ensures that ψ_B has proper bosonic symmetry under the exchange of two bosons. The fermionic wave function ψ_F is compactly written in a form of the Slater determinant,

$$\psi_F(x_1, \ldots, x_N, t) = \frac{1}{\sqrt{N!}} \det_{m,j=1}^{N} [\psi_m(x_j, t)], \tag{5}$$

where $\psi_m(x,t)$ denote N orthonormal single-particle (SP) wave functions obeying a set of uncoupled SP Schrödinger equations

$$i\frac{\partial \psi_m}{\partial t} = \left[-\frac{\partial^2}{\partial x^2} + V(x) \right]\psi_m(x,t), \quad m = 1, \ldots, N. \tag{6}$$

Equations (3)–(6) prescribe the construction of the many-body wave function describing the TG gas in an external potential $V(x)$, in both the static [1] and time-dependent [11] cases. The eigenstates of the TG system are

$$\psi_B(x_1, \ldots, x_N) = A(x_1, \ldots, x_N)\frac{1}{\sqrt{N!}} \det_{m,j=1}^{N} [\phi_m(x_j)], \tag{7}$$

where $\phi_m(x)$ are single-particle eigenstates for the potential $V(x)$. In the rest of the paper we will discuss the eigenstates of the TG system and their observables; hence, we drop the time variable from subsequent notation.

The many-body wave function ψ_B fully describes the state of the system. However, its form does not transparently yield physical information related to many important observables (e.g., the momentum distribution). The expectation values of one-body observables are readily obtained from the RSPDM, defined as

$$\rho_B(x,y) = N \int dx_2 \cdots dx_N \psi_B(x, x_2, \ldots, x_N)^*$$
$$\times \psi_B(y, x_2, \ldots, x_N). \tag{8}$$

The observables of great interest are the SP x density $\rho_B(x,x) = \sum_{m=1}^{N} |\phi_m(x)|^2$ and the momentum distribution [21]

$$n_B(k) = \frac{1}{2\pi} \int dx\, dy\, e^{ik(x-y)} \rho_B(x,y). \tag{9}$$

The SP density $\rho_B(x,x)$ is identical for the TG gas and the noninteracting Fermi gas [1]; however, the momentum distributions of the two systems considerably differ [21].

A concept that is very useful for the understanding of the many-body systems is that of natural orbitals. The NOs $\Phi_i(x)$ are eigenfunctions of the RSPDM,

$$\int dx \rho_B(x,y)\Phi_i(x) = \lambda_i \Phi_i(y), \quad i = 1, 2, \ldots, \tag{10}$$

where λ_i are the corresponding eigenvalues; the RSPDM is diagonal in the basis of NOs,

$$\rho_B(x,y) = \sum_{i=1}^{\infty} \lambda_i \Phi_i^*(x) \Phi_i(y). \qquad (11)$$

The NOs can be interpreted as effective SP states occupied by bosons, where λ_i represents the occupancy of the corresponding NO [23]. The sum of the Fourier power spectra of the NOs is the momentum distribution

$$n_B(k) = \sum_{i=1}^{\infty} \lambda_i \widetilde{\Phi}_i^*(k) \widetilde{\Phi}_i(k), \qquad (12)$$

where $\widetilde{\Phi}_i(k)$ is the Fourier transform of $\Phi_i(x)$.

The RSPDM of the noninteracting fermionic system on the Fermi side of the mapping is

$$\rho_F(x,y) = \sum_{m=1}^{N} \phi_m^*(x) \phi_m(y); \qquad (13)$$

evidently, the SP eigenstates $\phi_m(x)$ are NOs of the fermionic system, with occupancy unity [23]. The fermionic momentum distribution is

$$n_F(k) = \sum_{m=1}^{N} \widetilde{\phi}_m^*(k) \widetilde{\phi}_m(k), \qquad (14)$$

where $\widetilde{\phi}_m(k)$ is the Fourier transform of $\phi_m(x)$.

The calculation of the TG momentum distribution is preceded by a calculation of $\rho_B(x,y)$, which we conduct according to the method described in Ref. [40]. If the RSPDM is expressed in terms of the SP eigenstates ϕ_m as

$$\rho_B(x,y) = \sum_{i,j=1}^{N} \phi_i^*(x) A_{ij}(x,y) \phi_j(y), \qquad (15)$$

it can be shown that the $N \times N$ matrix $\mathbf{A}(x,y) = \{A_{ij}(x,y)\}$ has the form

$$\mathbf{A}(x,y) = (\mathbf{P}^{-1})^T \det \mathbf{P}, \qquad (16)$$

where the entries of the matrix $\mathbf{P}$ are $P_{ij}(x,y) = \delta_{ij} - 2\int_x^y dx' \phi_i^*(x') \phi_j(x')$ ($x < y$ without loss of generality) [40]. Formulas (15) and (16) enable fast numerical calculation of the RSPDM (and related quantities) for dark soliton states.

III. DS STATES ON THE RING

Within this section we analyze the RSPDM, the momentum distribution, and NOs and their occupancies for excited eigenstates of a TG gas on the ring of length L; in other words, the external potential is zero, x space is $x \in [-L/2, L/2]$, and periodic boundary conditions are imposed. The many-body eigenstates of the TG gas are constructed from the SP eigenstates of the system via Eq. (7). The SP eigenstates for the ring geometry are plane waves $\sqrt{1/L} e^{ik_m x}$, with SP energy k_m^2; here, $k_m = 2\pi m/L$ and m is an integer [48]. Apparently, the eigenstates $\sqrt{1/L} e^{ik_m x}$ and $\sqrt{1/L} e^{-ik_m x}$ are degenerate. This degeneracy in the SP eigenstates induces [via Eq. (7)] degeneracy of the TG many-body excited eigenstates. One particular subspace of degenerate eigenstates (DEs) is spanned with

$$\phi_m(x) = \frac{1}{\sqrt{L}}[a_m^- e^{-ik_m x} + a_m^+ e^{ik_m x}], \qquad (17)$$

where $|a_m^-|^2 + |a_m^+|^2 = 1$ and $m = 1, \ldots, N$; the corresponding many-body eigenstates are

$$\psi_{DE} = \frac{A(x_1, \ldots, x_N)}{\sqrt{N!}} L^{-N/2} \det_{j,m=1}^{N} [a_m^- e^{-ik_m x_j} + a_m^+ e^{ik_m x_j}]. \qquad (18)$$

Intuition suggests that, although these states are degenerate, some of the corresponding observables, such as the SP density in x space, the momentum distribution, spatial coherence, or entropy, could be quite different from one eigenstate to another depending on their internal symmetry, which is designated by the choice of the coefficients a_m^- and a_m^+.

In Ref. [11], Girardeau and Wright have pointed out that if one constructs excited many-body eigenstates of the TG gas on the ring as

$$\psi_{DS} = \frac{A(x_1, \ldots, x_N)}{\sqrt{N!}} \left(\frac{2}{L}\right)^{N/2} \det_{j,m=1}^{N} [\sin k_m x_j], \qquad (19)$$

that is, if one chooses the coefficients as $a_m^- = i/\sqrt{2}$ and $a_m^+ = -i/\sqrt{2}$, the SP density of these many-body eigenstates [11],

$$\rho_{DS}(x,x) = \frac{N+1}{L} - \frac{\sin\left(\dfrac{(N+1)2\pi x}{L}\right) \cos\left(\dfrac{N2\pi x}{L}\right)}{L \sin\left(\dfrac{2\pi x}{L}\right)}, \qquad (20)$$

has a structure closely resembling dark solitons [11] (hence the notation ψ_{DS} for the many-body wave function and analogously for related observables below). The structure of these excited eigenstates is somewhat artificial because on the fermionic side of the mapping, these states correspond to noninteracting fermions being placed solely within the *odd* SP eigenstates $\sin k_m x$. Nevertheless, such states can be excited by filtering of the many-body wave function [13].

Let us utilize the procedure outlined in Sec. II to calculate the RSPDM and related one-body observables for DS states [Eq. (19)]. It is straightforward to calculate the entries of the matrix $\mathbf{P} = 1 - \mathbf{Q}$ [see Eq. (16)], where

$$Q_{ij} = \frac{\sin[2(i+j)\pi x/L]}{(i+j)\pi} - \frac{\sin[2(i-j)\pi x/L]}{(i-j)\pi}$$
$$- \frac{\sin[2(i+j)\pi y/L]}{(i+j)\pi} + \frac{\sin[2(i-j)\pi y/L]}{(i-j)\pi}, \quad i \neq j,$$

$$Q_{ii} = -2\frac{x-y}{L} + \frac{\sin\left(\dfrac{4i\pi x}{L}\right)}{2i\pi} - \frac{\sin\left(\dfrac{4i\pi y}{L}\right)}{2i\pi}, \qquad (21)$$

for $i,j = 1, \ldots, N$. As for the inverse of the matrix $\mathbf{P}$, and consequently the RSPDM, we were able to find its analytical form up to $N=7$ by using Mathematica. However, for larger N we resorted to numerical calculations. It is straightforward
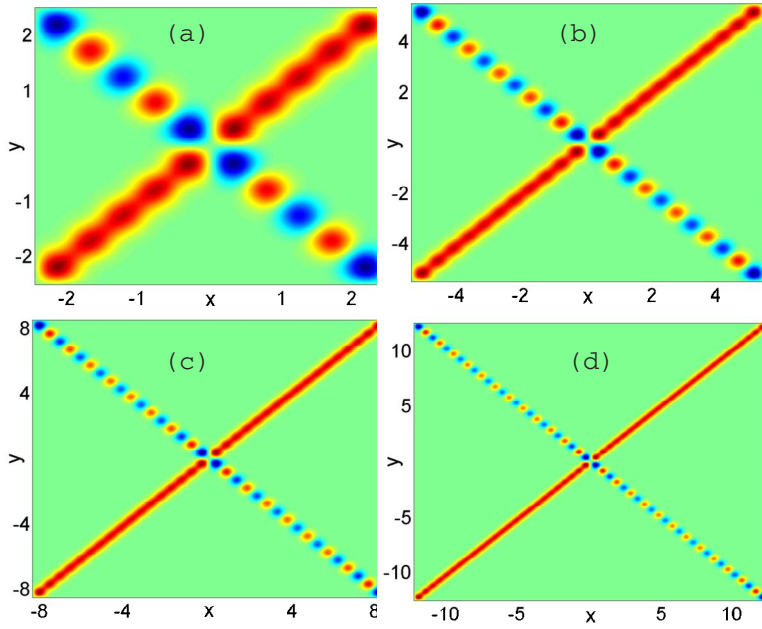
FIG. 1. (Color online) The RSPDM of dark soliton states, $\rho_{DS}(x,y)$, for $N=5$ (a), 11 (b), 17 (c), and 25 (d).

to see that the RSPDMs of two DS states, for two different values of L—say, L_1 and L_2—are connected by a simple scaling,

$$L_1\rho_{DS,L_1}(xL_1,yL_1) = L_2\rho_{DS,L_2}(xL_2,yL_2), \qquad (22)$$

where $x,y \in \left[-\frac{1}{2},\frac{1}{2}\right]$; thus, it is sufficient to calculate it for just one value of L. In what follows, without losing any generality, we choose $N=L$.

Figure 1 displays contour plots of $\rho_{DS}(x,y)$ for $N=5$, 11, 17, and 25. We clearly see a characteristic pattern for each value of N: The RSPDMs are largest close to the diagonal, with oscillations following the x-space density from Eq. (20). However, there are strong correlations along the line $x=-y$, indicating coherence between mirror points x and $-x$ around the DS center (at $x=0$).

Figure 2(a) displays the momentum distribution $n_{DS}(k)$ of DS states for $N=11$, 17, and 25. All momentum distributions for the ring geometry are normalized as $\Sigma_{k_m} n_B(k_m)=N$ (the SP momentum values k_m are discrete in the ring geometry). The momentum distributions have a characteristic shape with a smooth hump close to the origin ($k=0$) and with two sharp spikes which are located at $\pm k_{peak}=\pm\Sigma_{m=1}^N k_m/N=\pm\pi(N+1)/L$; the spikes indicate that there is a high probability of finding a boson in momentum states $\exp[\pm i\pi(N+1)/L]$. Note that due to our choice $N=L$, the peaks for different values of N approximately coincide at $\pm\pi(1+1/N)\approx\pm\pi$.

The sharp spikes at $\pm k_{peak}=\pm\pi(N+1)/L$ are intimately related to the strong correlations observed at the mirror points x and $-x$. This is illustrated in Fig. 3 which shows the cross-diagonal section of the RSPDM $\rho_{DS}(x,-x)$ and the function $\cos(2k_{peak}x)$ for $N=25$. There is evident correlation between $\rho_{DS}(x,-x)$ and $\cos(2k_{peak}x)$. Because of the symmetry $\rho_{DS}(x,y)=\rho_{DS}(y,x)$, the Fourier transform (FT) with respect to $\exp[ik(x-y)]$ reduces to FT with respect to $\cos k(x-y)$, which is $\cos 2kx$ at $y=-x$; hence, from Fig. 3 it immediately follows that the cross-diagonal behavior of $\rho_{DS}(x,-x)$ induces the peaks in the momentum distribution of DS states. We would like to point out that the correlations $\rho_{DS}(x,-x)$ do not decay, but oscillate, as the separation between points x and $-x$ is increased.

In order to gain more insight into the origin of the two sharp spikes in the momentum distribution and the related coherence between mirror points x and $-x$, it is illustrative to calculate the RSPDM and the momentum distribution for eigenstates that are degenerate (i.e., that have the same energy) to DS states, but which are less restrictive with respect to symmetry of the coefficients a_m^- and a_m^+. If the coefficients
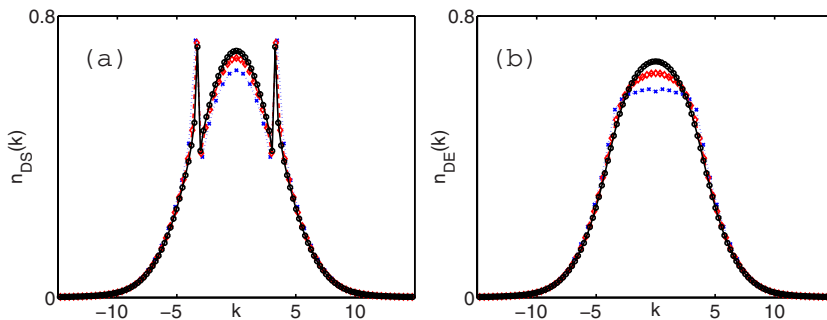

FIG. 2. (Color online) The momentum distributions corresponding to DS states (a) and to degenerate eigenstates with randomly chosen phases (b); figures are shown for $N=11$ ($\times$ symbols, blue dotted line), 17 (diamonds, red dashed line), and 25 (circles, solid black line).
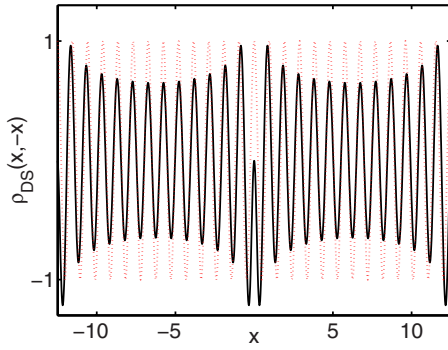
FIG. 3. (Color online) The cross-diagonal $\rho_{DS}(x,-x)$ of the dark soliton RSPDM (solid black line), displaying long-range oscillatory correlations between mirror points x and $-x$, and the cosine function $\cos(2k_{peak}x)$ (red dotted line).

are chosen as $a_m^- = i\exp(-i\theta_m)/\sqrt{2}$ and $a_m^+ = -i\exp(i\theta_m)/\sqrt{2}$, one obtains a whole class of eigenstates degenerate to dark solitons, which have the form

$$\psi_{DE} = \frac{A(x_1,\ldots,x_N)}{\sqrt{N!}}\left(\frac{2}{L}\right)^{N/2}\det_{j,m=1}^{N}[\sin(k_m x_j + \theta_m)], \quad (23)$$

where θ_m, $m=1,\ldots,N$ are N phases (for $\theta_m=0$, $\psi_{DS}=\psi_{DE}$).

Figure 4 displays contour plots of RSPDMs $\rho_{DE}(x,y)$, which corresponds to some typical states ψ_{DE} obtained from Eq. (23) by randomly choosing N phases θ_m (with respect to the uniform probability density in $[-\pi,\pi]$). We see that the SP density for this state, $\rho_{DE}(x,x)$, is not zero at $x=0$, which evidently follows from the fact that $\sin(k_m x + \theta_m)$ is not an odd function for $\theta_m \neq 0$, while $\rho_{DE}(x,x) = \Sigma_{m=1}^{N}|\sin(k_m x + \theta_m)|^2$. Furthermore, we observe that the structure of the RSPDM along the $x=-y$ line is absent; that is, there is no coherence between the mirror points x and $-x$. A closely related observation is that the momentum distributions of
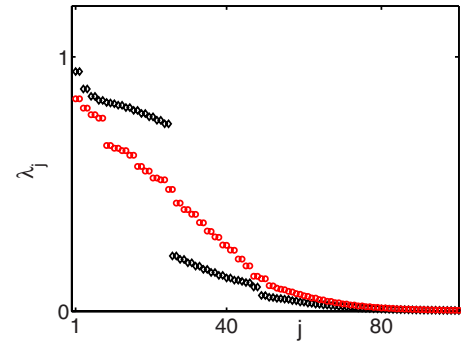

FIG. 5. (Color online) The occupancies of the NOs for the state ψ_{DS} (black diamonds) and a typical state ψ_{DE} (red squares), for $N=25$ particles. The sharp drop in the occupancies of ψ_{DS} occurs between λ_N and λ_{N+1}.

such states do not have a pair of sharp spikes which are present in $n_{DS}(k)$; this is illustrated in Fig. 2(b) which shows typical momentum distributions $n_{DE}(k)$ for $N=11$, 17 and 25.

Besides the RSPDM and the momentum distribution, excited many-body eigenstates of interest can be characterized by the corresponding NOs and their occupancies. Figure 5 shows the occupancies of the NOs of the state ψ_{DS} and a typical state ψ_{DE} for $N=25$. We observe that the occupancies are fairly low (less than 1) for all NOs, but there is a sharp drop in the occupancies after the 25th (Nth) NO for the DS state. We have observed such a behavior for other values of N as well. In contrast, the occupancies of the NOs corresponding to a typical state ψ_{DE} do not exhibit a sharp drop after the Nth orbital, but decrease rather smoothly.

Figure 6 illustrates the spatial structure and the Fourier power spectra of the NOs corresponding to the DS state for $N=25$. The spatial structure of calculated NOs is either symmetric or antisymmetric. This is connected to the symmetry $\rho_{DS}(x,y)=\rho_{DS}(-y,-x)$; due to this symmetry, it follows that if some NO is nondegenerate, it is either symmetric or anti-
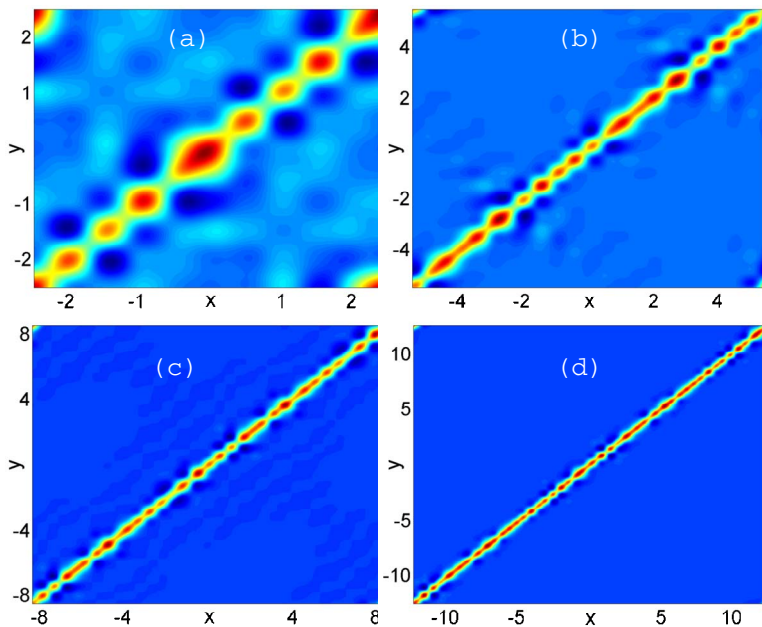

FIG. 4. (Color online) The RSPDM of typical eigenstates ψ_{DE} [Eq. (23)] for $N=7$ (a), 11 (b), 17 (c), and 25 (d).
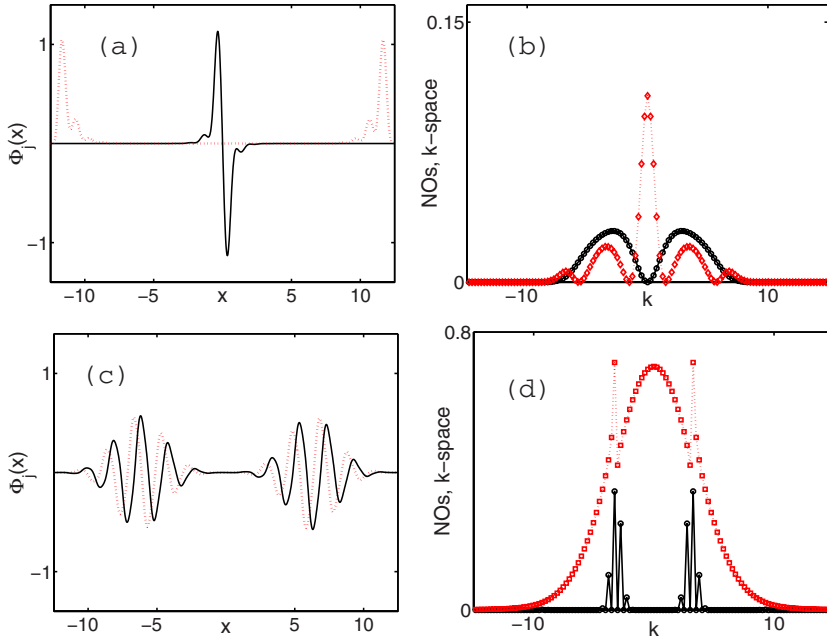
FIG. 6. (Color online) The NOs of a DS state in x space (left column) and their power spectra in k space (right column) for $N=25$. (a) The first $\Phi_1(x)$ (black solid line) and third $\Phi_3(x)$ (red dotted line) NOs. (b) The Fourier power spectrum of the first $|\tilde{\Phi}_1(k)|^2$ (black circles, solid line) and third $|\tilde{\Phi}_3(k)|^2$ (red diamonds, dotted line) NOs. (c) The 24th (red dotted line) and 25th (black solid line) NOs in x space. (d) The momentum distribution (red squares, dotted line) in comparison to the contribution from the 24th and 25th NOs: $\Sigma_{i=24}^{25}\lambda_i|\tilde{\Phi}_i(k)|^2$ (black circles, solid line).

symmetric; if two NOs are degenerate (their occupancies are identical), they can be superimposed to yield one symmetric and one antisymmetric NO. Our numerical study shows that the low-order (leading) NOs are localized in space, but broad in k space; Fig. 6(a) depicts the x-space structure, and Fig. 6(b) show the k-space structure of the first and third NOs. We see that these low-order NOs do not contribute to the sharp peaks observed in the momentum distribution of DS states. Further inspection of the NOs reveals that those NOs just on the upper side of the sharp drop in λ_j (Fig. 5) are in fact responsible for the sharp peaks: Figures 6(c) and 6(d) display the x-space and k-space structures, respectively, of the 24th and 25th NOs ($N=25$). The total momentum distribution [red squares, dotted line in Fig. 6(d)] can be written as $\Sigma_{i=1}^{\infty}\lambda_i\tilde{\Phi}_i^*(k)\tilde{\Phi}_i(k)$; a contribution to this sum stemming from the 24th and 25th NOs is shown in Fig. 6(d) with black solid line. Evidently, for this DS state where $N=25$, the 24th and 25th NOs give rise to the peaks in the momentum distribution.

It is interesting to note that when all phases are chosen to be $\theta_m=\pi/2$, then all of the fermionic NOs are $\propto\cos(k_m x)$, and we again observe a higher degree of correlation between mirror points in the RSPDM and peaks in the momentum distribution (not shown).

All of the observations above indicate a somewhat smaller degree of order in the degenerate eigenstates ψ_{DE} than in dark solitons ψ_{DS}, which follows from the random (disordered) choice of the phases θ_m. This is further underpinned in Table I, which shows the entropy $S=-\Sigma_i p_i \ln p_i$, where $p_i=\lambda_i/N$, for the dark soliton states ψ_{DS} and typical ψ_{DE} states. The entropy of states ψ_{DE} is systematically larger than in the states ψ_{DS}.

From our observations it follows that the many-body state ψ_{DS} contains a distinct component, which can be interpreted as a standing wave populating momentum modes at $\pm k_{peak}$. In the effective single-particle picture, we see that this component gives rise to the population of the natural orbitals

close to (and including) the Nth NO. However, it should be pointed out that this component is fairly small; i.e., it yields a small occupation of these effective SP states.

In a similar fashion to the excited ψ_{DS} state, the ground state of the TG gas on the ring yields a distinct population of the zero-momentum mode [21]; in this case, however, the zero-momentum mode is the leading natural orbital and its population is fairly large (it scales as $\sqrt{N}$ [28]). Even though the TG states are not Bose condensed, they can sharply populate a single-momentum mode because bosons do not obey the Pauli principle and consequently more than one boson can occupy a single-momentum state (which is not the case for noninteracting fermions).

It is interesting to note that on the Fermi side of the mapping, the momentum distribution of noninteracting fermions $n_F(k)$ is uniform up to the Fermi edge (excluding the zero-momentum mode at $k_0=0$) and does not depend on the randomly chosen phases θ_m:

$$n_{F,DS}(k_m) = n_{F,DE}(k_m) = \begin{cases} \dfrac{1}{2} & \text{if } 1 \leqslant |m| \leqslant N \\ 0 & \text{otherwise.} \end{cases} \tag{24}$$

Namely, the SP eigenstates $\sin(k_m x + \theta_m)$ are NOs of the fermionic system. The Fourier power spectrum of each SP state $\sin(k_m x + \theta_m)$ [which determine the fermionic momentum distribution via Eq. (14)] does not depend on the phase θ_m. Each

TABLE I. The entropy S of dark soliton states and typical ψ_{DE} states for different values of the number of particles N.

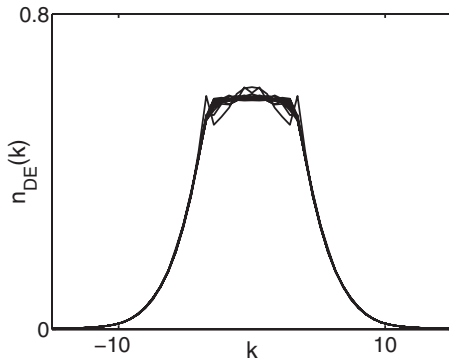| N	$S[\psi_{DS}]$	$S[\psi_{DE}]$
11	2.90	3.21
17	3.39	3.66
25	3.83	4.05

FIG. 7. Momentum distributions for ten different states ψ_{DE} [Eq. (23)] chosen at random, by randomly choosing ten sets $\{\theta_m | m = 1, \ldots, N\}$ of phases (see text for details).

fermionic NO $\sin(k_m x + \theta_m)$ can be written as a superposition of two plane waves $\sin(k_m x + \theta_m) = (e^{ik_m x + i\theta_m} - e^{-ik_m x - i\theta_m})/2i$. Evidently, the mean value of the momenta pointing in the positive [negative] direction is $\pi(N+1)/L$ $[-\pi(N+1)/L]$; that is, it is identical to k_{peak}. When the fermionic states are mapped to the TG states, a wave function component which distinctively populates momentum modes at $\pm k_{peak}$ can appear. This occurs when the phases θ_m act coherently; i.e., it is evident that a random choice of the phases θ_m destroys the observation of the two spikes connected with this component.

Before closing this section we should say that in all our numerical calculations, the phases of the states ψ_{DE} were chosen at random (with respect to the uniform probability density in $[-\pi, \pi]$). A random choice of the phases yields a typical state ψ_{DE} in the sense that one-body observables, such as the momentum distribution, of typical states approximately coincide. In order to verify this assumption Fig. 7 displays momentum distributions for ten eigenstates ψ_{DE}

($N=11$ particles), obtained by ten randomly chosen configurations $\{\theta_m | m = 1, \ldots, N\}$ of the phases. The momentum distribution only slightly varies from case to case with one exception that exhibits two (relatively small) dark solitonic spikes. Exceptions from the typical behavior will be harder to see for larger values of N, because in this case the parameter space spanned by N phases θ_m is larger and it is harder to correlate the phases by chance, which could yield characteristic solitonic spikes in the momentum distribution. Hence, we can conclude that our observations regarding the class of states ψ_{DE} from Eq. (23) hold for practically all of these states in the sense stated above.

IV. DS STATES IN A PARITY-INVARIANT WELL-SHAPED POTENTIAL

The concept of dark solitons can be extended to various types of parity-invariant potentials (e.g., see [13]). DS states are found in harmonic confinement [12] periodic lattices [13], well-shaped potentials [13], and so-forth. In Ref. [13] it was shown that by parity invariant filtering of the many-body wave function one could in principle excite the TG gas into a DS state. Let us compare the RSPDM and the momentum distribution of DS states on the ring and in a parity-invariant potential $V_c(x) = V_c^0 \{2 + \Sigma_{i=1,2}(-)^{i+1} \tanh x_w [x + (-)^i x_c]\}$ ($V_c^0 = 15$, $x_w = 8$, and $x_c = 25$). In such a potential, DS states are constructed by populating the first N odd SP eigenstates on the Fermi side of the map. Figure 8(a) displays the RSPDM, while Fig. 8(b) displays the momentum distribution of such an excited eigenstate for $N=10$. We clearly observe that the structure of the RSPDM and the momentum distribution is similar to that of DS states on the ring; the RSPDM has off-diagonal mirror-point correlations, while the momentum distribution has two sharp spikes. Furthermore, Fig. 8(c) displays the occupancies of the NOs, which clearly exhibit a large and sudden drop after the Nth NO. Figure 8(d) shows
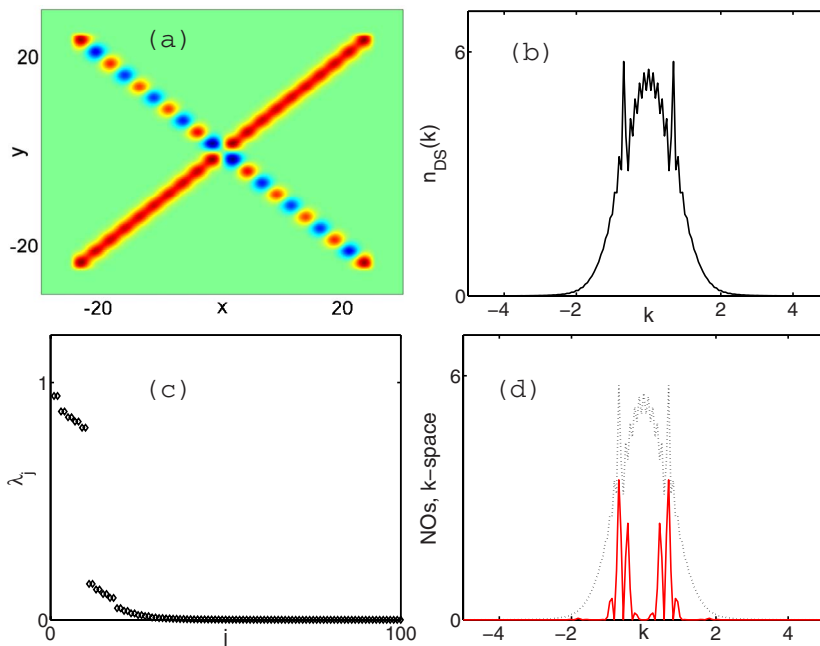

FIG. 8. (Color online) The RSPDM (a), momentum distribution (b), and occupancies of the NOs (c) for a DS state ($N=10$) in a parity-invariant well-shaped potential. (d) The momentum distribution (black dotted line) in comparison to the contribution from the ninth and tenth NOs: $\Sigma_{i=9}^{10} \lambda_i |\tilde{\Phi}_i(k)|^2$ (red solid line).

the contribution from the $(N-1)$th and Nth NOs to the momentum distribution: $\Sigma_{i=9}^{10}\lambda_i\widetilde{\Phi}_i^*(k)\widetilde{\Phi}_i(k)$; clearly, these NOs are responsible for the peaks in the momentum distribution.

The observations presented in Fig. 8 suggest that the behavior of the one-body observables of DS states, such as the two sharp spikes in the momentum distribution and correlation between the mirror points in the RSPDM, can be found in various types of parity-invariant potentials.

V. CONNECTION TO INCOHERENT LIGHT

We would like to point out that the behavior of incoherent light in linear [49] and nonlinear [50–53] optical systems has many similarities to the behavior of interacting (partially condensed or noncondensed) Bose gases [13,53–55]. The dynamics of incoherent light in nonlinear systems attracted considerable interest in the past decade since the first experiments on incoherent solitons [50] in noninstantaneous nonlinear media were conducted. A number of important results were obtained (for a review, e.g., see Ref. [51]) since then. Among the recent results one finds, e.g., the experimental observation of incoherent solitons nonlinear photonic lattices [52] and thermalization of incoherent nonlinear waves [53]. We believe that many of the phenomena observed with incoherent light in optics [50–53] can find their counterpart in the context of Bose gases.

In Ref. [13] it has been pointed out that there is mathematical relation between the propagation of partially spatially incoherent light in *linear* 1D photonic structures and quantum dynamics of a TG gas. More specifically, the correlation functions describing incoherent nondiffracting beams in optics [49] can be mapped [13] to DS states. However, it should be emphasized that the spatial power spectrum of these incoherent beams corresponds to the momentum distribution of noninteracting fermions; i.e., it profoundly differs from the momentum distribution of DS states in a TG gas discussed here.

VI. SUMMARY

We have employed a recently obtained formula [40] to numerically calculate the RSPDM correlations, natural orbitals and their occupancies, and the momentum distribution of dark solitons in a TG gas. We have found that these excited eigenstates of a TG gas have characteristic shape of the momentum distribution, which has two distinguished sharp spikes; while most of the paper is devoted to the ring geometry, where the spikes are located at $k_{peak}=\pm\pi(N+1)/L$ (N is the number of particles and L is the length of the ring), we have shown results which suggest that such behavior is general for DS states in parity-invariant potentials. It has been shown that the spikes in the momentum distribution are closely connected to the cross-diagonal oscillatory long-range correlations between mirror points (x and $-x$) in the RSPDM. This behavior of DS states follows from the fact that they are specially tailored; in the ring geometry, it has been shown that the two spikes and a special form of spatial coherence are lost for most eigenstates that are degenerate to DS states.

[1] M. Girardeau, J. Math. Phys. **1**, 516 (1960).
[2] E. Lieb and W. Liniger, Phys. Rev. **130**, 1605 (1963); E. Lieb, *ibid.* **130**, 1616 (1963).
[3] F. Schreck, L. Khaykovich, K. L. Corwin, G. Ferrari, T. Bourdel, J. Cubizolles, and C. Salomon, Phys. Rev. Lett. **87**, 080403 (2001); A. Görlitz, J. M. Vogels, A. E. Leanhardt, C. Raman, T. L. Gustavson, J. R. Abo-Shaeer, A. P. Chikkatur, S. Gupta, S. Inouye, T. Rosenband, and W. Ketterle, *ibid.* **87**, 130402 (2001); M. Greiner, I. Bloch, O. Mandel, T. W. Hansch, and T. Esslinger, *ibid.* **87**, 160405 (2001); H. Moritz, T. Stöferle, M. Kohl, and T. Esslinger, *ibid.* **91**, 250402 (2003); B. Laburthe Tolra, K. M. O'Hara, J. H. Huckans, W. D. Phillips, S. L. Rolston, and J. V. Porto, *ibid.* **92**, 190401 (2004); T. Stöferle, H. Moritz, C. Schori, M. Kohl, and T. Esslinger, *ibid.* **92**, 130403 (2004).
[4] T. Kinoshita, T. Wenger, and D. S. Weiss, Science **305**, 1125 (2004).
[5] B. Paredes, A. Widera, V. Murg, O. Mandel, S. Fölling, I. Cirac, G. V. Shlyapnikov, T. W. Hänsch, and I. Bloch, Nature (London) **429**, 277 (2004).
[6] T. Kinoshita, T. Wenger, and D. S. Weiss, Nature (London) **440**, 900 (2006).
[7] In the limit of infinitely strong δ-function interactions, the Lieb-Liniger gas becomes a gas of impenetrable bosons in 1D—i. e., the TG gas.
[8] M. Olshanii, Phys. Rev. Lett. **81**, 938 (1998).
[9] D. S. Petrov, G. V. Shlyapnikov, and J. T. M. Walraven, Phys. Rev. Lett. **85**, 3745 (2000).
[10] V. Dunjko, V. Lorent, and M. Olshanii, Phys. Rev. Lett. **86**, 5413 (2001).
[11] M. D. Girardeau and E. M. Wright, Phys. Rev. Lett. **84**, 5691 (2000).
[12] T. Busch and G. Huyet, J. Phys. B **36**, 2553 (2003).
[13] H. Buljan, O. Manela, R. Pezer, A. Vardi, and M. Segev, Phys. Rev. A **74**, 043610 (2006).
[14] S. Burger, K. Bongs, S. Dettmer, W. Ertmer, K. Sengstock, A. Sanpera, G. V. Shlyapnikov, and M. Lewenstein, Phys. Rev. Lett. **83**, 5198 (1999); J. Denschlag *et al.*, Science **287**, 97 (2000).
[15] R. Dum, J. I. Cirac, M. Lewenstein, and P. Zoller, Phys. Rev. Lett. **80**, 2972 (1998).
[16] Th. Busch, and J. R. Anglin, Phys. Rev. Lett. **84**, 2298 (2000).
[17] A. E. Muryshev, G. V. Shlyapnikov, W. Ertmer, K. Sengstock, and M. Lewenstein, Phys. Rev. Lett. **89**, 110401 (2002).
[18] E. B. Kolomeisky, T. J. Newman, J. P. Straley, and Xiaoya Qi, Phys. Rev. Lett. **85**, 1146 (2000).
[19] D. J. Frantzeskakis, N. P. Proukakis, and P. G. Kevrekidis

Phys. Rev. A **70**, 015601 (2004).

[20] M. Ögren, G. M. Kavoulakis, and A. D. Jackson, Phys. Rev. A **72**, 021603(R) (2005).

[21] A. Lenard, J. Math. Phys. **5**, 930 (1964); T. D. Schultz, *ibid.* **4**, 666 (1963); H. G. Vaidya and C. A. Tracy, *ibid.* **42**, 3 (1979).

[22] D. B. Creamer, H. B. Thacker, and D. Wilkinson, Phys. Rev. D **23**, 3081 (1981); M. Jimbo and T. Miwa, *ibid.* **24**, 3169 (1981).

[23] M. D. Girardeau, E. M. Wright, and J. M. Triscari, Phys. Rev. A **63**, 033601 (2001); G. J. Lapeyre, M. D. Girardeau, and E. M. Wright, *ibid.* **66**, 023606 (2002).

[24] A. Minguzzi, P. Vignolo, and M. P. Tossi, Phys. Lett. A **294**, 222 (2002).

[25] M. A. Cazalilla, Europhys. Lett. **59**, 793 (2002).

[26] M. Olshanii and V. Dunjko, Phys. Rev. Lett. **91**, 090401 (2003).

[27] T. Papenbrock, Phys. Rev. A **67**, 041601(R) (2003).

[28] P. J. Forrester, N. E. Frankel, T. M. Garoni, and N. S. Witte, Phys. Rev. A **67**, 043607 (2003).

[29] D. M. Gangardt and G. V. Shlyapnikov, Phys. Rev. Lett. **90**, 010401 (2003).

[30] G. E. Astrakharchik and S. Giorgini, Phys. Rev. A **68**, 031602(R) (2003).

[31] M. Rigol and A. Muramatsu, Phys. Rev. A **70**, 031603(R) (2004).

[32] D. M. Gangardt, J. Phys. A **37**, 9335 (2004).

[33] G. P. Berman, F. Borgonovi, F. M. Izrailev, and A. Smerzi, Phys. Rev. Lett. **92**, 030404 (2004).

[34] M. Rigol and A. Muramatsu, Phys. Rev. Lett. **94**, 240403 (2005).

[35] A. Minguzzi and D. M. Gangardt, Phys. Rev. Lett. **94**, 240404 (2005).

[36] J. Brand and A. Yu. Cherny, Phys. Rev. A **72**, 033619 (2005).

[37] P. J. Forrester, N. E. Frankel, and M. I. Makin, Phys. Rev. A **74**, 043614 (2006).

[38] D. M. Gangardt and G. V. Shlyapnikov, New J. Phys. **8**, 167 (2006).

[39] M. Rigol, V. Dunjko, V. Yurovsky, and M. Olshanii, Phys. Rev.

[40] R. Pezer and H. Buljan, Phys. Rev. Lett. **98**, 240403 (2007).

[41] F. Deuretzbacher, K. Bongs, K. Sengstock, and D Pfannkuche, Phys. Rev. A **75**, 013614 (2007).

[42] J.-S. Caux, P. Calabrese, and N. A. Slavnov, J. Stat. Mech. J. Stat. Mech.: Theory Exp. 2007, P01008 (2007).

[43] Y. Lin and B. Wu, Phys. Rev. A **75**, 023613 (2007).

[44] J. G. Muga and R. F. Snider, Phys. Rev. A **57**, 3317 (1998).

[45] K. Sakmann, A. I. Streltsov, O. E. Alon, and L. S. Cederbaum, Phys. Rev. A **72**, 033613 (2005).

[46] M. T. Batchelor, X.-W. Guan, N. Oelkers, and C. Lee, J. Phys. A **38**, 7787 (2005).

[47] The behavior of the *discrete* HCB-lattice model is not fully equivalent to the TG model in a *continuous* potential; e.g., see M. A. Cazalilla, Phys. Rev. A **70**, 041604(R) (2004).

[48] For simplicity, here we focus only on an odd number of particles on the ring. If N is even, then $k_m = 2\pi m/L + \pi/L$ and m is integer (see footnote 6 in Ref. [2]).

[49] J. Turunen, A. Vasara, and A. T. Friberg, J. Opt. Soc. Am. A **8**, 282 (1991); A. V. Shchegrov and E. Wolf, Opt. Lett. **25**, 141 (2000).

[50] M. Mitchell, Z. Chen, M. Shih, and M. Segev, Phys. Rev. Lett. **77**, 490 (1996); M. Mitchell and M. Segev, Nature (London) **387**, 880 (1997); Z. Chen, M. Mitchell, M. Segev, T. Coskun, and D. N. Christodoulides, Science **280**, 889 (1998).

[51] M. Segev and D. N. Christodoulides, in *Incoherent Solitons in Spatial Solitons*, edited by S. Trillo and W. Torruellas (Springer, Berlin, 2001), pp. 87–125.

[52] O. Cohen, G. Bartal, H. Buljan, J. W. Fleischer, T. Carmon, M. Segev, and D. N. Christodoulides, Nature (London) **433**, 500 (2005).

[53] S. Pitois, S. Lagrange, H. R. Jauslin, and A. Picozzi, Phys. Rev. Lett. **97**, 033902 (2006); for a recent review, see A. Picozzi, Opt. Express **15**, 9063 (2007), and references therein.

[54] M. Naraschewski and R. J. Glauber, Phys. Rev. A **59**, 4595 (1999).

[55] H. Buljan, M. Segev, and A. Vardi, Phys. Rev. Lett. **95**, 180401 (2005).

Lett. **98**, 050405 (2007).